Characterization of X-ray radiation from solid Sn target irradiated by femtosecond laser pulses in the presence of air plasma sparks

A. CURCIO,[1,2] M. ANANIA,[1] F.G. BISESTO,[1,2] A. FAENOV,[3,4] M. FERRARIO,[1] M. GALLETTI,[1] D. GIULIETTI,[5] R. KODAMA,[3,6] M. PETRARCA,[7,8] T. PIKUZ,[3,4] AND A. ZIGLER[1,9]

[1]INFN National Laboratories of Frascati, Frascati, Italy
[2]Physics Department of the Roma University "La Sapienza", Rome, Italy
[3]Institute for Academic Initiatives, Osaka University, Suita, Osaka, 565-0871, Japan
[4]Joint Institute for High Temperatures, Russian Academy of Sciences, ul. Izhorskaya 13/19, Moscow 125412, Russia
[5]Physics Department of the University and INFN, Pisa, Italy
[6]PPC Osaka University and JST, CREST, 2-1, Yamadaoka, Suita, Osaka 565-0871, Japan
[7]S.B.A.I. department of the Roma University "La Sapienza", Rome, Italy
[8]INFN Roma1, Rome, Italy
[9]Racah Institute of Physics, Hebrew University, Jerusalem 91904, Israel

Abstract

The emission of X-rays from solid tin targets irradiated by low-energy (few mJ) femtosecond laser pulses propagated through air plasma sparks is investigated. The aim is that to better understand the X-ray emission mechanism and to show the possibility to produce proper radiation for spectroscopic and imaging applications with a table-top laser system. The utilization of a controlled ultrashort prepulse is found necessary to optimize the conversion efficiency of laser energy into L_α radiation. The optimum contrast between the main pulse and the controlled prepulse is found about 10^2. A correlation between the laser contrast value and the laser near-infrared spectra at the exit of the plasma spark is observed.

Keywords: Air plasma sparks; X-rays; Femtosecond laser

1. INTRODUCTION

The interaction of an ultrashort laser pulse with a gas target offers a wide variety of physical phenomena, due to the complex interaction between the laser and the electrons of the generated plasma. The particular interaction is determined by the adopted interaction scheme, by the laser system parameters and the environment parameters. The interest in gas targets grew up dramatically in the last decades, especially due to the non-linear optics applications. Just to cite some of them: laser wakefields generation (Tajima & Dawson, 1979; Mangles *et al.*, 2006; Malka *et al.*, 2008), harmonic generation in gases (Franken *et al.*, 1961), pulse compression (Lange *et al.*, 1998), beam filamentation (Braun *et al.*, 1995), terahertz radiation generation (Hoyer *et al.*, 2005), and light coherent scattering (Mitryukovskiy *et al.*, 2013). In the present work, the generation of L_α line from air plasma sparks in front of a metal target is studied, following (Pikuz *et al.*, 2010) where K_α emission was used to perform micro-radiographies. Based on (Nagao *et al.*, 2004; Faenov *et al.*, 2010; Ledingham *et al.*, 2011; Zhidkov *et al.*, 2012), we optimized the X-ray radiation from a thick (2 mm) tin (Sn) target, by moving the target relative to the laser focus in the presence of the air plasma spark. In addition, at each point we conducted a scan by varying the energy ratio between the main pulse and a controlled prepulse. The laser energy was varied in order to characterize the efficiency of such a setup as X-ray source. Finally, spectral measurements in the near-infrared range have been done, by varying again the laser contrast, with the goal to find a correlation with the X-ray signals. The striking aspect of this experiment is that of producing several keV photons in air with a table-top laser system, 3 mJ in 50 fs, corresponding to 60 GW power. For air plasma sparks density and temperature parameters, typically $\sim 10^{16} cm^{-3}$ and several eV (Zhang *et al.*, 2012), the

---

Address correspondence and reprint requests to: A. Curcio, INFN National Laboratories of Frascati, Frascati, Italy. E-mail: alessandro.curcio@lnf.infn.it

presence of keV electrons, responsible for the X-ray emission from metal, is not expected. The presence of the plasma spark, composed by air plasma and metal surface plasma, is the environment where the electrons are accelerated, producing X-ray radiation when they are damped inside the solid density region of the Sn target. The ablation depth of a metal target in atmosphere is found to be much smaller than in vacuum (Di Bernardo *et al.*, 2003), due to the atmospheric pressure, which prevents the formation of big craters by redeposition mechanisms. The plasma expansion from the metal surface in this configuration is strongly inhibited (Chen *et al.*, 2013). The direct laser–solid target interaction is also affected in atmosphere by the effect of the plasma defocusing due to the strong ionization occurring meanwhile the laser is tightly focused in air. The expected laser intensity in vacuum is such that X-rays in the keV region could be observed from the interaction with the solid target, nevertheless keV photons are unexpected when the interaction occurs in air. In previous works (Faenov *et al.*, 2010; Ledingham *et al.*, 2011; Zhidkov *et al.*, 2012), kHz repetition laser were used showing a higher efficiency in the number of yield K_α X-ray photons. This could be due at least to two reasons: the first is the higher efficiency of K_α line production with respect to L_α line through electron inelastic scattering inside metals; the second is related to the air refraction index properties, which on the millisecond scale can bring memory from the previous pulse to the next giving birth to focusing effects in some cases, increasing and maintaining the laser intensity over many Rayleigh lengths (Jhajj *et al.*, 2014). The correlation showed in the last section of the present paper between X-ray signals and near-infrared signals can lead to a better interpretation of the phenomenon under analysis, related to an efficient multi-photon ionization of the air plasma.

2. EXPERIMENTAL METHOD AND RESULTS

The experiment consisted in three parts: plasma extension characterization through a visible charge-coupled device (CCD) camera, X-ray spectra detection through an X-ray CCD camera in single-photon counting mode, near-infrared spectroscopy through a fiber spectrometer. The experimental setup is shown in Figure 1.

We used a Ti:Sa (0.8 μm central wavelength) 3 mJ, 50 fs laser split in polarization through a half-wave plate, which ensures the adjustability of the energy ratio between the controlled prepulse and the main pulse (the contrast), and a polarizing beam splitter. The intrinsic contrast of the laser system is 10^9, preventing us to have more than one significant prepulse. The overall elongation of the laser pulse inside the glass of the optical elements is compensated through a pre-chirp induced in the compression phase. The main pulse and the prepulse are separated by 0.5 ns. The plasma lifetime for the plasma generated by the controlled prepulse is expected to be about 10 ns (Couairon & Mysyrowicz, 2007). In this way, the main pulse interacts with a preformed plasma. A telescope is mounted in order to increase the beam diameter

up to 4 cm before the final 20 cm focal length lens. Given our parameters, the expected laser beam diameter inside the air plasma channel is expected to be some tens of microns. This average value typically comes out from the compensation of many focusing/defocusing effects, such as initial lens focusing, plasma defocusing, diffraction, and pre-plasma focusing. The CCD-X camera is at ∼ 5 cm from the Sn target. The CCD-X line of sight forms an $\pi/6$ angle with the laser beam impinging on the target. The X-ray radiation is attenuated during the free propagation in air and also by the passage through a 75 μm Kapton window put on the entrance of a short flange mounted in front of the CCD sensors in order to keep them to −20°C, so lowering the electronic noise. In front of the sensors is also applied a composed thin filter 4 μm PoliPropylene plus 0.4 μm aluminum, useful to screen the visible–infrared radiation coming from the interaction point.
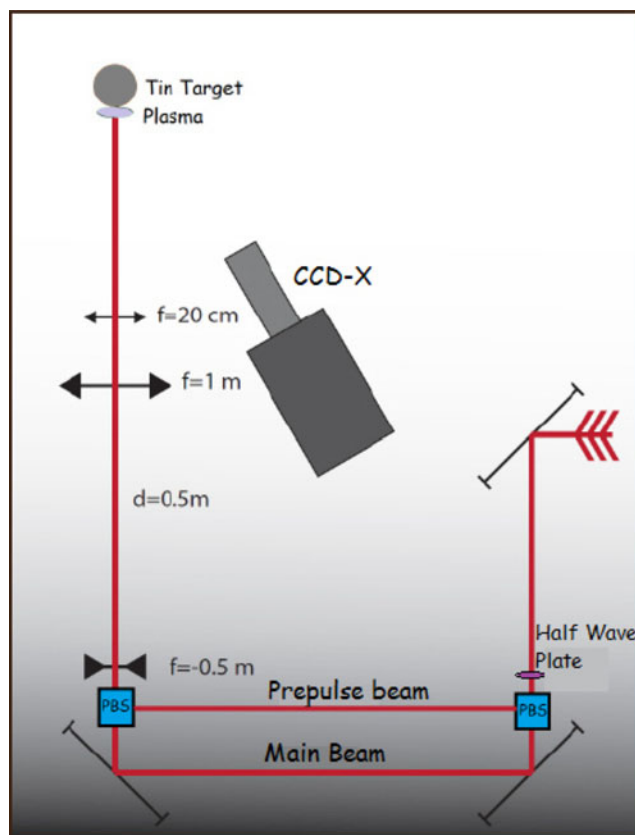

Fig. 1. Experimental setup: the laser beam starts from the right, and then it passes through a half-wave plate in order to distribute the laser energy into the s- and p-polarizations in a controlled way. After this, the laser is split in polarization by a polarizing beam splitter. The delay line between the main pulse and the prepulse is 0.5 ns. A telescope is mounted with the goal to increase the beam diameter at the entrance of the last focusing lens. The two pulses are focused in air by a 20 cm positive lens. The air plasma is formed in front of the Sn target. When target is moved along the spark X-rays are observed and detected by a CCD-X in single-photon counting mode.

2.1. Plasma extension

The measured plasma longitudinal extension was 700 μm, as in Figure 2a and 2b. This parameter turned to be important in the phase of focus-scan, where the Sn target was moved along the plasma channel. Figure 2b shows the air plasma extension, namely without the target. Nevertheless during the interaction the plasma composition and evolution is strongly affected by the presence of the target, in fact the overall plasma is a mixture of air plasma and metal surface plasma. In this environment, electrons are accelerated to some keV, inducing X-ray radiation when decelerating inside the solid density region.

2.2. X-ray detection and characterization

The X-ray spectra were detected in single-photon counting mode, taking into account in the analysis the effect of CCD-X quantum efficiency, the air absorption, the Kapton window and the aluminated-plastic filter. First a focus-scan was made moving the Sn target along the plasma spark in order to find the best point of interaction, yielding the maximum number of L_α photons. In Figure 3a–3c, the results are reported. In particular, Figure 3a and 3b show the formation of L_α line and the yielded number of photons when varying the distance of the solid target from an optimum point marked as zero. The negative (positive) sign indicates the negative (positive) sense of moving, namely toward (in the same vs. of) the impinging laser. The number $dN/d\Omega dE$ of
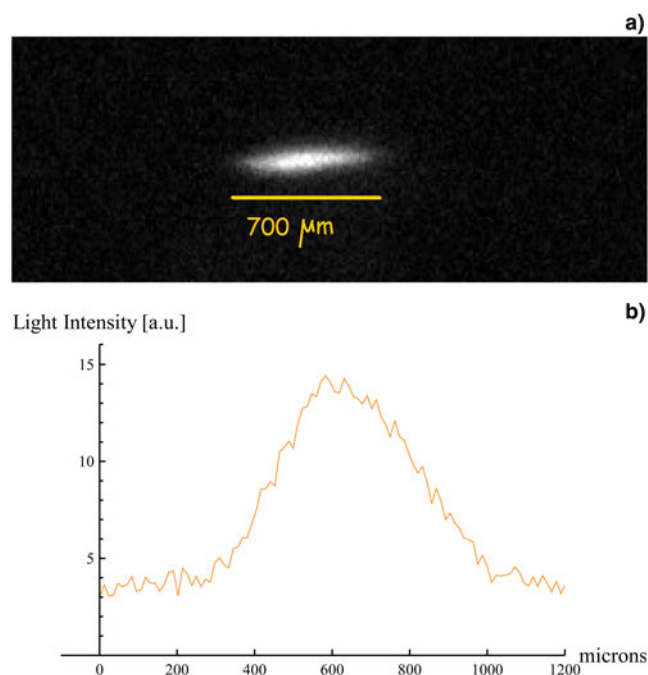
photons per unit solid angle and unit energy emitted by the source per each laser shot is reported.

A fine scan was then performed with 10 μm steps in the proximity of the optimum point. The optimum point was found around the center of the spark as in (Zhidkov *et al.*, 2012), where the plasma is a mixture of air plasma and metal surface plasma. The number of L_α photons, that is, the number of photons emitted in the region of the Sn L_α

Fig. 2. (a) Spectral and temporal integrated plasma light: longitudinal profile of the plasma spark. (b) Line-out of the longitudinal profile of the plasma spark.
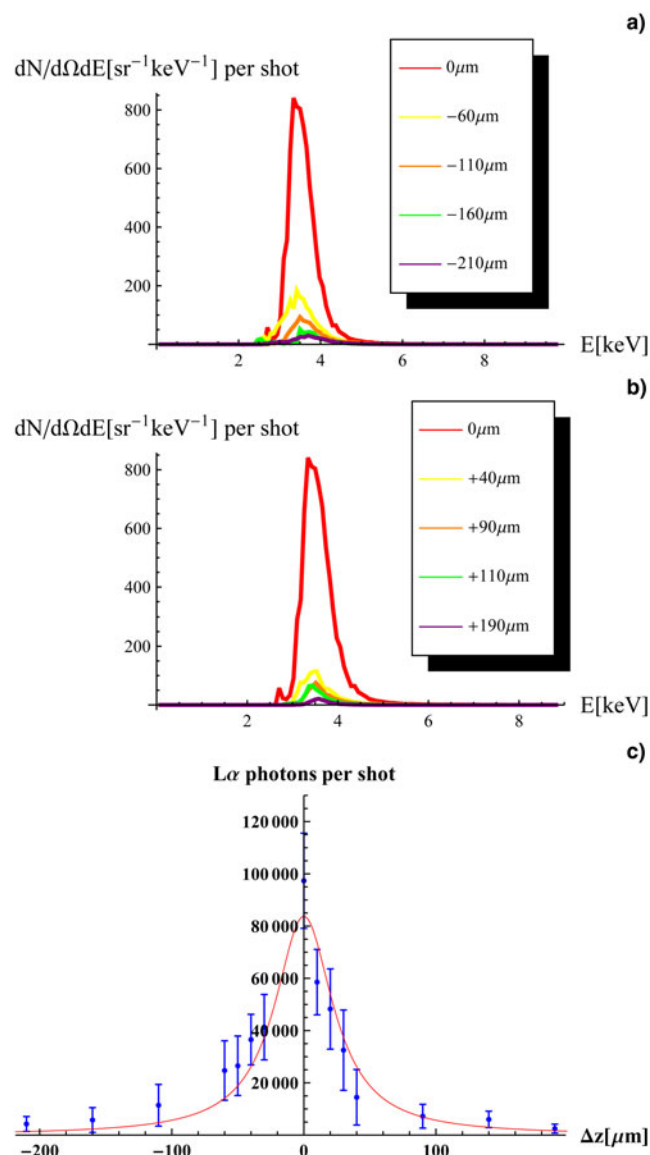

Fig. 3. (a) X-ray spectra for different negative (toward the incoming laser) positions of the Sn target inside the plasma channel with respect to the optimum point taken as the origin of the displacements. The optimum point is found in the center of the plasma spark. (b) X-ray spectra for different positive (in the same vs. of the incoming laser) positions of the Sn target inside the plasma channel with respect to the optimum point taken as the origin of the displacements. The optimum point is found in the center of the plasma spark. (c) Summary of the focus-scan results. FWHM width of the Lorentzian fit $\Delta z = 27$ μm. The spectral and angular integrated number of L_α photons is reported with respect to the position of the target inside the plasma spark.

nominal energy 3.44 keV, per shot emitted from the target along the plasma channel is showed in Figure 3c together with a Lorentzian fit. The full wifth half maximum (FWHM) of the fit curve is found $\Delta z = 27$ μm, less than a tenth the plasma extension length. It means that significant changes in the number of L_α photons could be observed only outside a region of about 2 Δz around the optimum interaction point. The second part of the X-ray analysis consisted in characterizing the L_α radiation with respect to the controlled contrast. The Sn target was fixed in the previously found optimum position and the contrast was adjusted trough the half-wave plate in front the first Polarizing Beam Splitter (PBS) (see Fig. 1) in such a way to work with contrasts between 1 and 100. In order to work with higher contrasts, suitable neutral density filters were adopted on the prepulse line. The results are showed in Figure 4a and 4b. The presence of a prepulse seems to be fundamental when looking to Figure 4b where is showed that the maximum yielded radiation is obtained for contrast between 10^1 and 10^2, while for the lower and higher contrast value the number of photons decays rapidly. For higher contrasts the L_α emission is strongly suppressed probably due to the fact that the prepulse fluence falls under the damage threshold of the metal (about $1\ J/cm^2$), making impossible the formation of a composed air–metal plasma profile.
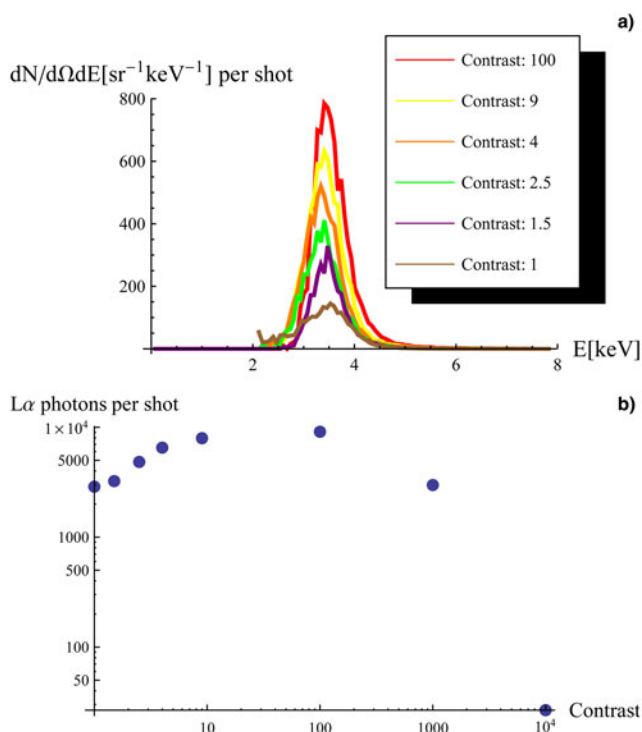

Fig. 4. (a) X-ray spectra for different contrast value. The target is positioned in the optimum point for the yield L_α photons, and then with the help of the half-wave plate the energy ratio between the main pulse and the prepulse is adjusted. (b) Number of L_α photons versus laser contrast. The target is positioned in the optimum point for the yield L_α photons. The spectral and angular integrated number of L_α photons is reported with respect to the energy ratio (contrast) between the main pulse and the prepulse.
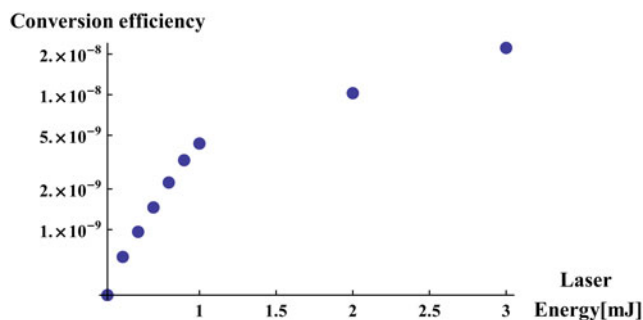

Fig. 5. Conversion efficiency of the laser energy into L_α radiation. The target position and the contrast between the main pulse and the controlled prepulse are chosen in such a way to optimize the yield L_α photons. The ratio between the energy irradiated at the L_α line and the laser energy is reported for different values of the laser energy.

The final part of the X-ray detection study consisted in the characterization of our system as X-ray source. The conversion efficiency from the laser energy to L_α radiation was studied for different values of the laser energy. The contrast was fixed at 10^2 and the target was in the zero (optimum) position. The result is shown in Figure 5, and it is referred like in Figure 3c and 4b to the number of photons emitted from the Sn target. The L_α radiation production is very low for energies approximating to some hundreds of μJ probably because of the 10^2 contrast, which makes the prepulse to be not efficient in modifying the air index refraction. It is worth noting that in previous works K_α radiation was found even for laser energy around some tens of μJ, working with a kHz high repetition laser (Faenov *et al.*, 2010; Pikuz *et al.*, 2010; Zhidkov *et al.*, 2012). Even if in these works no punctual mention is given about the laser contrast, the K_α production in the same configuration seems to be more efficient.

2.3. Correlation between X-ray and near-infrared spectra

We have demonstrated the correlation between the near-infrared spectra and the X-ray spectra when the laser contrast is adjusted. The spectra were detected at the exit of the plasma channel without the Sn target. We showed that by varying the ratio between the artificial prepulse and the main pulse a significant blue-shift of the self-modulated laser radiation is obtained for ratios approaching to the optimum contrast 10^2 (Fig. 4b). If varying the contrast value in the region $10^1 - 10^2$ where the maximum L_α production efficiency was found, no significant change in the blue-shifted spectra were registered (Fig. 6). This demonstrates the existence of a parameters region where the laser intensity reaches a maximum value independent from the energy ratio between the prepulse and the main pulse. Previous works demonstrated that blue-shifts of some tens of nanometers can be related to efficient multi-photon ionization, and a constant shift can be related to a fixed laser intensity (Giulietti & Giulietti, 2015
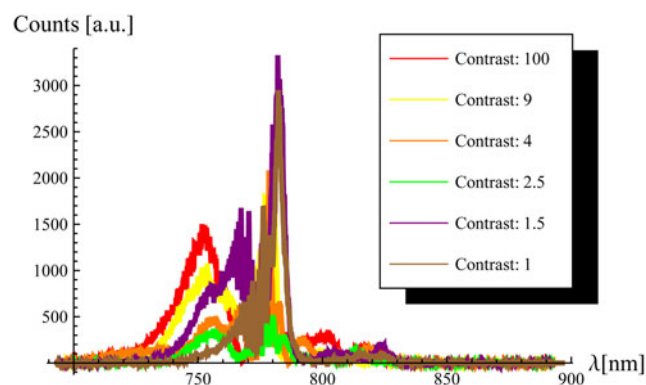
Counts [a.u.]

Fig. 6. Near-infrared laser spectra at the exit of the plasma channel for different contrast values.

and references therein; Koga *et al.*, 2000). This leads to the conclusion that the role of the prepulse is in modifying the index of refraction of the air plasma, determining a maximum intensity for the main pulse capable to interact with the air–Sn plasma accelerating electrons up to many keV.

3. CONCLUSIONS

The characterization of L_α radiation from air plasma sparks in front of an Sn target was performed by using a Ti:Sa, 3 mJ, 50 fs laser. The focal scan showed the existence of a narrow 27 µm region in which the production of radiation is more efficient. The contrast scan showed that the presence of 1% of the laser energy ultrashort prepulse is required to obtain optimum conversion efficiency to L_α radiation. At this level of prepulse, above the damage threshold of the metal, the laser–electron interaction occurs in a region where the plasma composition is determined by the air plasma and the metal surface plasma. The near-infrared spectroscopy points out the influence of the ionization process in air by ultrashort prepulse on the focusing of the main laser pulse on metal target. The correlation found between the laser contrast value and the laser near-infrared spectra at the exit of the plasma spark, without the solid target, could be an indirect diagnostic method for the optimization of the X-ray flux when the target is inserted in the setup.

ACKNOWLEDGEMENTS

REFERENCES

Braun, A., Korn, G., Liu, X., Du, D., Squier, J. & Mourou, G. (1995). Self-channeling of high-peak-power femtosecond laser pulses in air. *Opt. Lett.* **20**, 73–75.

Chen, Z., Wu, Q., Yang, M., Tang, B., Yao, J., Rupp, R.A., Cao, Y. & Xu, J. (2013). Generation and evolution of plasma during femtosecond laser ablation of silicon in different ambient gases. *Laser Part. Beams* **31**, 539–545.

Couairon, A. & Mysyrowicz, A. (2007). Femtosecond filamentation in trasparent media. *Phys. Rep.* **44**, 47–109.

Di Bernardo, A., Courtois, C., Cros, B., Matthieussent, G., Batani, D., Desai, T., Strati, F. & Lucchini, G. (2003). High-intensity ultrashort laser-induced ablation of stainless steel foil targets in the presence of ambient gas. *Laser Part. Beams* **21**, 59–64.

Faenov, A.Ya., Pikuz, S.A., Zidkov, A.G., Skobelev, I.Yu., Komarov, P.S., Chefonov, O.V., Gasilov, S.V. & Ovchinnikov, A.V. (2010). Excitation of X-rays by electrons accelerated in air in the wake wave of a laser pulse. *JETP Lett.* **92**, 375.

Franken, P.A., Hill, A.E., Peters, C.W. & Weinreich, G. (1961). Generation of optical harmonics. *Phys. Rev. Lett.* **7**, 118.

Giulietti, A. & Giulietti, D. (2015). Self-phase modulation in various regimes of intense laser-plasma interactions. *J. Plasma Phys.* **81**, 495810608.

Hoyer, W., Knorr, A., Moloney, J.V., Wright, E.M., Kira, M. & Koch, S.W. (2005). Photoluminescence and terahertz emission from femtosecond laser-induced plasma channels. *Phys. Rev. Lett.* **94**, 115004.

Jhajj, N., Rosenthal, E.W., Birnbaum, R., Wahlstrand, J.K. & Milchberg, H.M. (2014). Demonstration of long-lived high-power optical waveguides in air. *Phys. Rev. X* **4**, 011027.

Koga, J.K., Naumova, N., Kando, M., Tsintsadze, L.N., Nakajima, K., Bulanov, S.V., Dewa, H., Kotaki, H. & Tajima, T. (2000). Fixed blueshift of high intensity short pulse lasers propagating in gas chambers. *Phys. Plasmas* **7**, 5223–5228.

Lange, H.R., Ripoche, L.F., Chiron, A.A., Lamouroux, B., Franco, M.A., Prade, B. & Mysyrowicz, A. (1998). Time-space self-compression of femtosecond laser pulses in air. In *Quantum Electronics Conference, 1998. IQEC 98. Technical Digest. Summaries of papers presented at the International* (pp. 243–244). IEEE.

Ledingham, K.W.D., Abuazoum, S.S., McCanny, T., Melone, J.J., Spohr, K., Schramm, U., Kraft, S.D., Wagner, A. & Jochmann, A. (2011). Comparison of hard X-ray production from various targets in air using a short pulse kHz laser with photon production from a high power multifilament laser beam from the same targets in air. *arXiv:*1106.4152[physics.plasm-ph].

Malka, V., Faure, J., Gauduel, Y.A., Lefebvre, E., Rousse, A. & Ta Phuoc, K. (2008). Principles and Applications of compact laser-plasma accelerators. *Nat. Phys.* **4**, 447–453.

Mangles, S., Walton, B. & Najmudin, N., Dangor, A.E., Krushelnik, K., Malka, V., Manclossi, M., Lopes, N., Carias, C., Mendes, G. & Dorchies, F. (2006) Table-top laser–plasma acceleration as an electron radiography source. *Laser Part. Beams* **24**, 185–190.

Mitryukovskiy, S.I., Liu, Y., Prade, B., Houard, A. & Mysyrowicz, A. (2013). Coherent synthesis of terahertz radiation from femtosecond laser filaments in air. *Appl. Phys. Lett.* **102**, 221107.

Nagao, H., Hironaka, Y., Nakamura, K.G. & Kondo, K. (2004). Hard X-ray emission from a copper target by focussing a picosecond laser beam at 3×10^{13} W/cm^2. *Jap. J. Appl. Phys.* **43**, 1207–1208.

Pikuz, S.A., Chefonova, O.V., Gasilova, S.V., Komarova, P.S., Ovchinnikova, A.V., Skobeleva, I.Yu., Ashitkova, S.Yu., Agranata, M.V., Zigler, A. & Faenov, A.Ya. (2010). Microradiography with laser plasma X-ray source operating in air atmosphere. *Laser Part. Beams* **28**, 393–397.

Tajima, T. & Dawson, J. (1979). Laser electron accelerator. *Phys. Rev. Lett.* **43**, 267.

Zhang, N., Wu, Z., Xu, K. & Zhu, X. (2012). Characteristics of micro air plasma produced by double femtosecond laser pulses. *Opt. Express* **20**, 2528–38. doi: 10.1364/OE.20.002528.

Zhidkov, A.G., Pikuz, S.A., Faenov, A.Ya., Chefonov, O.V., Ovchinnikov, A.V., Agranat, M.B. & Zigle, A. (2012). Generation of hard X-rays by femtosecond laser pulse interaction with solid targets in atmosphere. *Opt. Lett.* **37** 884–886.